Open Access

Journal of Energy and Power Technology

LIDSEN Publishing Inc.

Original Research

TEA of a Unique Two-Pathways Process for Post-Combustion CO_2 Capture

Rui Wang [1], Husain E. Ashkanani [2], Bingyun Li [3], Badie I. Morsi [1,*]

1. Department of Chemical and Petroleum Engineering, University of Pittsburgh, Pittsburgh, PA 15261, USA; E-Mails: ruw28@pitt.edu; morsi@pitt.edu
2. Department of Chemical Engineering, College of Engineering and Petroleum, Kuwait University, P.O. Box 5969, Safat 13060, Kuwait; E-Mail: husain.ashkanani@ku.edu.kw
3. Department of Orthopaedics, School of Medicine, West Virginia University, Morgantown, WV 26506, USA; E-Mail: bili@hsc.wvu.edu

* **Correspondence:** Badie I. Morsi; E-Mail: morsi@pitt.edu

Academic Editors: Nagasree Garapati and Megan Smith

Special Issue: Carbon Dioxide Utilization: Strategies for an Evolving Climate

Journal of Energy and Power Technology
2022, volume 4, issue 4
doi:10.21926/jept.2204033

Received: August 01, 2022
Accepted: October 07, 2022
Published: October 13, 2022

Abstract

A unique two-Pathways process using aqueous sodium glycinate for CO_2 capture from a split flue gas stream emitted from 600 MWe post-combustion coal power plant was developed in Aspen Plus v.10. The split gas flow rate used was 44.75 ton/h and contained 0.0023 mol% SO_2 and 13.33 mol% CO_2. The process includes a washing unit, a CO_2 absorption unit, a reverse osmosis unit, and a solvent regeneration unit or an ultrafiltration unit. The washing unit uses deionized water to completely remove SO_2 and the CO_2 absorption unit uses SGS to capture at least 90 mol% of the CO_2 in the split flue gas stream. Upon CO_2 and SGS reactions, the resulting liquid products exhibit phase-separation into CO_2-lean phase and CO_2-rich phase, allow two distinct pathways. Pathway (i) is to regenerate mostly the CO_2-rich phase, collect the released CO_2, and compress it for sequestration purposes. Pathway (ii) is to send the liquid stream from the CO_2 absorption unit to the ultrafiltration unit to separate the solid nanomaterials. The hydraulics and mass transfer characteristics in the washing and CO_2 absorption units were obtained; and techno-economic analysis (TEA) for Pathways (i) and (ii),

including Capital Expenditure (CAPEX), Operating Expenditure (OPEX), and Levelized Cost of CO_2 Captured (LCOC), were calculated and compared. The simulation results revealed that the CAPEX, OPEX, and LCOC for Pathway (i) were ($12,039,251), (261 $/h), and (54.01 $/ton-$CO_2$ captured), respectively, and those for Pathway (ii) were ($5,908,000), (237.2 $/h), and (39.90 $/ton-$CO_2$ captured), respectively. Moreover, in Pathway (ii), 8.19 ton/h of CO_2 were captured to produce 15.62 ton/h $NaHCO_3$ nanomaterials, which were sold to offset the overall process cost. The LCOC values indicate that Pathway (ii) is more cost-effective than Pathway (i) because LCOC values for Pathway (ii) are much lower than those for Pathway (i).

Keywords
CO_2 capture; sodium glycinate; packed-bed absorber; hydraulics; techno-economic analysis

1. Introduction

The atmospheric emissions of naturally occurring greenhouse gases (GHGs), including carbon dioxide (CO_2), methane (CH_4), nitrous oxide (N_2O), and water vapor (H_2O), and synthetically-made GHGs, such as chlorofluorocarbons (CFCs), are increasing the global average temperature, which has already reached 1°C above the pre-industrial level [1]. The increase of the global temperature due to atmospheric GHGs emissions has disastrous impacts on humans and the environment [2]. For instance, it will lead to: (1) melting of glaciers and ice in polar regions and rising of sea level, which could flood several worldwide coastal areas, leading to forced migration, hunger, and loss of human lives [3]; (2) warming and changing of the ocean chemistry, which could disrupt the ocean ecosystem and food web, resulting in dramatic consequences on marine species, and lifestyle of humans depending on them [4, 5]; and (3) increasing the intensity and frequency of cyclones, hurricanes, precipitation, and storm surge, leading to loss of human lives and infrastructure, dangerous floods, severe droughts and intolerable heatwaves [6].

The recent rise of the global temperature is due in part to the unmanageable global CO_2 emissions, which have increased from 22.8 Gt (Gigaton = 10^9 ton) in 1998 to 34.0 Gt in 2019 [7]. Table 1 shows CO_2 emissions from fuel combustion in 2019 [8, 9], and as can be seen the largest share of CO_2 emission comes from electricity and heat production plants at (41.2%), transportation (including aviation, navigation, cars, rails and pipelines transport) at (24.1%), small industries at (18.5%), buildings at (8.2%), and others at (8.0%), totaling 34.0 Gt.

Table 1 CO_2 emissions from fuel combustion in 2019 [8, 9].

CO_2 emission source	**Gigaton (Gt)**	**Share of total**
Electricity and heat production plants	14.0	41.2%
Transportation, including aviation, navigation, cars, rail and pipeline transport	8.2	24.1%
Industry	6.3	18.5%
Buildings	2.8	8.2%
Others	2.7	8.0%

Total (Gt)	34.0	100%

On the effort to mitigate global average temperature rise, the 2015-Paris Agreement on climate change aimed at holding the temperature rise to well below 2°C and to pursue endeavors to limit this rise to 1.5°C [10, 11]. In 2018, the Intergovernmental Panel on Climate Change (IPCC) projected that by 2030, the CO_2 emission has to decrease by 25% or 45% to limit the average global temperature to below 2°C or below 1.5°C, respectively [12]. To curb the CO_2 emissions into atmosphere, worldwide preventative and mitigative strategies have been implemented. Preventive strategies include programs, which are directly related to promoting the use of renewable energies and improving energy efficiency, while mitigative strategies refer to CO_2 emission controls from power plants and industrial facilities, which discharge huge amounts of CO_2 into the atmosphere. The European Union (EU) Strategic Energy Technology (SET) predicts that Carbon Capture and Sequestration (CCS) will contribute up to 30% of the total CO_2 emission reduction in EU by 2050 [13]. Ketzer, Iglesias [14] also estimated that the CCS may contribute to 20% of global CO_2 emission reduction by 2050 and to 55% by 2100.

Due to their different chemical properties, GHGs are removed from the atmosphere by various processes, e.g., CO_2 is absorbed by sinks, such as live plants, soil, and the ocean, however, CFCs are only destroyed by sunlight in the upper atmosphere. In 2020, the US-IEA reported that coal and natural gas were the major primary energy sources for the total global electricity generation at 38% and 23%, respectively [15]. To reduce the CO_2 emission from coal power plant, several CO_2 capture strategies are available, including pre-combustion, oxy-combustion, and post-combustion capture [16]. Despite the advantages of pre-combustion and oxy-fuel combustion captures, they are unlikely to replace post-combustion capture on a global scale [17] because the latter is capable of retrofitting with current gas turbine system [18]. Post-combustion capture technologies include using adsorbents, membranes, and chemical absorbents (solvents).

This paper is focusing on post-combustion CO_2 capture processes using only chemical solvents, while using membranes and solid adsorbents as post-combustion methods are beyond the scope of this study. Numerous chemical solvents have been used in post-combustion CO_2 capture processes, including aqueous ammonium hydroxide, potassium carbonate solutions, alkanolamines, and amino acids [19]. The Aqua-Ammonia process uses aqueous NH_4OH for CO_2 capture from flue gas. Darde, Thomsen [20] simulated CO_2 capture from flue gas using chilled ammonia at temperature between 275 and 283 K. Liu, Wang [21] measured the overall mass transfer coefficients of CO_2 in 5% and 10% aqueous ammonia at 293 K and 313 K in a small wetted-wall column. Jiang, Yu [22] also simulated the CO_2 absorption by aqueous ammonia in Aspen Plus and optimized the process using inter-cooling system in the absorber to enhance CO_2 absorption and improve the overall process.

The Benfield process employs hot potassium carbonate (K_2CO_3) solutions to capture CO_2 and H_2S from flue gas and natural gas [23]. This process was claimed to have several advantages, such as low regeneration energy, low volatility, multi-impurities capture (CO_2, SO_x, and NO_x), beside producing fertilizer [24, 25]. Smith, Xiao [26] designed a laboratory-scale pilot plant to capture 4-10 kg/h CO_2 from an air/CO_2 feed gas rate of 30-55 kg/h and developed an Aspen Plus model, which was validated against the pilot plant data. In addition, The Cooperative Research Center for Greenhouse Gas Technologies (CO2CRC) developed the UNO MK3 process, which used K_2CO_3 for capturing 90 % of the CO_2 emission in a large-scale power plant [26].

Aqueous monoethanolamine (MEA) is frequently used for CO_2 capture from flue gas and natural gas [19, 27-29]. The CO_2-MEA reaction is fast, however, the production of stable carbamates [30], leads to an average CO_2 loading capacity and a high solvent regeneration energy requirement [31, 32]. Godini and Mowla [33] constructed a pilot-scale plant using MEA, obtained different experimental data in a wide range of operating conditions, and developed a mathematical model, which was validated against the pilot plant experimental data. Diethanolamine (DEA) and triethanolamine have relatively low heat of reaction with CO_2 and accordingly they require low regeneration duty [34, 35], nonetheless, their CO_2 absorption rates are too slow to use without the addition of a promoter [32]. Methyl-diethanolamine (MDEA) was used for CO_2 capture from flue gas [36]. Sterically hindered amine (e.g., 2-amino-2-methyl-1-propanol aka AMP) was reported to have a good CO_2 loading and a reasonable absorption rate [32, 37-49]. Law, Azudin [50] also developed a model in Aspen Plus v8.8 to optimize the CO_2 capture process using MEA and MDEA blends.

Sodium glycinate salt (SGS), as an amino acid (AA), was used as an absorbent for CO_2 capture due to its high CO_2 loading, non-volatile nature, and resistance to degradation in gas streams containing oxygen [51-54]. Lee, Choi [55] measured the density, viscosity, surface tension of SGS solutions at different concentrations at temperatures between 303 and 353 K. Park, Son [56] investigated the reaction kinetics between CO_2 and SGS at different temperatures between 298 K and 318 K using a stirred semi-batch vessel. Lee, Song [57] simulated the CO_2 absorption by SGS with different concentrations and temperatures using Pro-II and the physical properties of SGS solution predicted by Pro-II model were compared with actual experimental data. Also, Vaidya, Konduru [58] studied the CO_2 reaction kinetics with two aqueous amino acids, potassium glycinate and taurine using a stirred-cell reactor. More recently, Li, Wang [59] experimentally demonstrated the formation of bicarbonate nanoflowers and nanofibers when using amino acid (AA)-XOH solutions to capture CO_2, wherein X stands for sodium (Na) or potassium (K) and AA are Glycine or Alanine.

The preceding introduction reveals the following: (1) numerous solvents have been used in post-combustion CO_2 capture processes at lab-scale and pilot-scale, however, the TEA of these processes are not available in the open literature; (2) it is impossible to compare the performance of the solvents used under similar operating conditions, including the same flue gas composition, which makes it difficult to select an effective solvent for CO_2 capture; and (3) even though AAs have been used for CO_2 capture, they were not used for producing high-value products, which could be sold to offset the cost of the CO_2 capture process.

The main objective of this study is to develop in Aspen Plus v.10 and perform techno-economic analysis (TEA) of a unique two-Pathways, post-combustion CO_2 capture process using SGS to remove CO_2 from a split stream from the flue gas emitted from the 600 MWe clean coal power plant, intended for use in the Wolverine Clean Energy Venture (WCEV) project. This process produces an aqueous CO_2-rich stream, including solid sodium bicarbonate ($NaHCO_3$) nanomaterials, which can be proceeded in two different Pathways (i) and (ii) as illustrated in Figure 1 . In Pathway (i), the CO_2-rich stream containing the solid nanomaterials is regenerated in a stripper and the released CO_2 is compressed in preparations for subsequent sequestration in geologic formation or for use in enhance oil recovery (EOR), considering the federal 45Q tax credits for CO_2 reduction are available at \$50/ton for sequestration and \$35/ton for EOR. In Pathway (ii), the $NaHCO_3$ solid nanomaterials, which have numerous uses [60-62], are separated from the CO_2-rich stream and could be sold to offset the overall costs of the CO_2 capture process. In addition, this pathway could be a novel venue for producing $NaHCO_3$, which is conventionally manufactured by the Solvay process or by mining

natron, a naturally occurring mineral consisting of sodium bicarbonate, sodium carbonate decahydrate ($Na_2CO_3 \cdot 10H_2O$) and small amounts of sodium chloride and sodium sulfate [63].

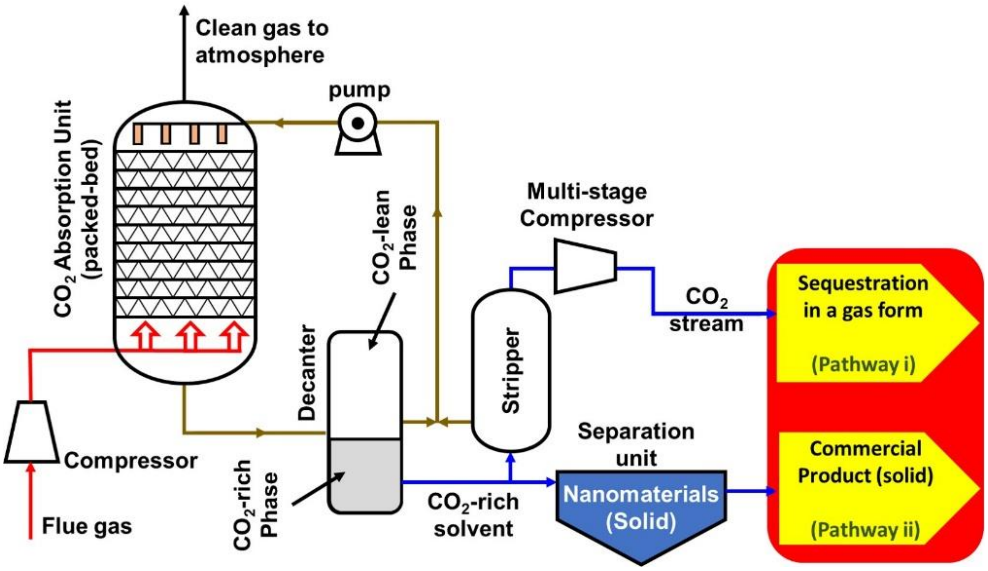

Figure 1 Process two Pathways.

It is important to mention that our two-Pathways process offers a great flexibility and a risk management strategy, however, market forces, including sequestration costs, product demand, and cost of electricity, would factor into the decision for selecting the desired pathway. Nonetheless, due to the huge daily atmospheric CO_2 emissions, Pathway (i) could be the main pathway to follow, while Pathway (ii) would be switched on when electricity is in high demand since CO_2 desorption in pathway (i) requires electricity.

2. Aspen Plus Simulation

Our chemical process simulation in Aspen Plus v.10 required, among other, precise knowledge of (1) The physico-chemical properties of the solute and solvent species, (2) The solute-solvent reaction kinetics, including reaction rate constants, and reaction orders with respect to the solute and the solvent; and (3) The design criteria of the unit operation to be used to carry out the chemical reactions, including flooding, gas-liquid mass transfer, two-phase pressure drop, liquid-phase holdup, and packing specific wetted area. It should be noted that the most common unit operation used in CO_2 capture is a counter-current packed-bed absorber. These will be discussed in the following.

2.1 Properties of the Flue Gas-Liquid Solvent Used

The composition of the flue gas from the Wolverine 600 MWe power plant used is given in Table 2; and the flow rate of the split flue gas stream used in this study was 12.43 kg/s (44.75 ton/h) at 353.15 K and 1.013 bar.

Table 2 Flue gas composition from the Wolverine 600 MW power plant [64].

Components	mol %	wt %
CO_2	13.33	20.18
H_2O	12.31	7.63
N_2	70.36	67.79
O_2	4.00	4.400
SO_2	2.35×10^{-3}	5.20×10^{-3}

Table 3 includes some properties of glycine and H_2O, which are available in Aspen Plus v.10 database, and those of SGS, which were reported by Lee, Song [57]. The properties of H_3O^+, Na^+, OH^- and HCO_3^- ions, which are present as result of the chemical reaction between CO_2 and SGS are also available in Aspen Plus database.

Table 3 Properties of H_2O, glycine and SGS [57].

Properties	**H_2O**	**Glycine**	**SGS**
Molecular weight, kg/kmol	18.01	75.07	97.05
Normal boiling point, K	373.20	699	541.54
Critical temperature, K	647.30	1,021	736.60
Critical pressure, MPa	22.05	6.74	4.27
Critical volume, m^3/kmol	0.06	0.20	0.35
Acentric factor, -	0.34	0.69	0.95
Heat of formation, kJ/mol	-241.84	-390.37	-372.54
Gibbs free energy of formation, kJ/mol	-228.61	-299.90	-188.23

The constraints imposed on our CO_2 capture process were: (1) 100 mol% SO_2 removal from the split flue gas stream in the WU before CO_2 absorption, (2) at least 90 mol% CO_2 capture from the desulfurized flue gas in the CAU, (3) no flooding in the process to ensure smooth operation, (4) the water content in the CO_2 stream destined for sequestration must be less than 600 ppm to avoid the formation of CO_2 ice-like hydrates in the transportation lines, and (5) the packing height to diameter (H/D) ratio for the packed-beds used should be equal or greater than 6 to avoid channeling in both units as previously reported in the literature [65, 66]. The existence of preferential flow pathways, aka, channeling instead of homogeneous flow is often observed when (H/D) ratio is <5 [67]. The presence of channeling substantially reduces the gas-liquid interfacial area and mass transfer, which lower the absorption efficiency of the CAU [68]. To completely remove SO_2, the raw flue gas is first washed in a WU using Deionized Water (DIW) in a counter-current packed-bed absorber wherein the reaction between SO_2 and H_2O takes place.

2.2 SO_2 Reaction with H_2O

The Henry's Law constants for CO_2, SO_2, N_2 and O_2 absorption into DIW are available in the literature [69]. Also, the ELEC-NRTL model in Aspen Plus includes the following reactions: water dissociation (R-1), CO_2 and water reaction to form bicarbonate ions (R-2), bicarbonate dissociation in water to form carbonate ions (R-3), SO_2 reaction with oxygen to form SO_3 (R-4), and SO_3 reaction

with water to form H_2SO_4 (R-5). All these are equilibrium reactions, and therefore their corresponding equilibrium rate constants can be calculated using the change of the standard Gibbs free energy (ΔG°) [70].

$$2H_2O \rightleftharpoons OH^- + H_3O^+ \Delta G^o = 79.91 kJ/mol, \quad \Delta H^o = 55.82 kJ/mol \qquad (R-1)$$

$$CO_2 + 2H_2O \rightleftharpoons H_3O^+ + HCO_3^- \Delta G^o = 36.36 kJ/mol, \quad \Delta H^o = 7.62 kJ/mol \qquad (R-2)$$

$$HCO_3^- + H_2O \rightleftharpoons CO_3^{2-} + H_3O^+ \Delta G^o = 58.97 kJ/mol, \quad \Delta H^o = 14.84 kJ/mol \qquad (R-3)$$

$$2SO_2 + O_2 \rightleftharpoons 2SO_3 \Delta G^o = -140.51 kJ/mol, \quad \Delta H^o = -196.95 kJ/mol \qquad (R-4)$$

$$SO_3 + H_2O \rightleftharpoons H_2SO_4 \Delta G^o = -136.77 kJ/mol, \quad \Delta H^o = -227.92 kJ/mol \qquad (R-5)$$

2.3 CO_2 Reactions with Aqueous SGS

As the simplest amino acid, glycine (NH_2CH_2COOH) undergoes zwitterionic transformation to protonate the amino group according to reaction (R-6) to become zwitterion glycine ($NH_3^+CH_2COO^-$), which does not react with CO_2 [71]. In the presence of NaOH, however, the amino group is deprotonated in this basic environment to form SGS (NH_2CH_2COONa), which is readily reactive with CO_2 as expressed in reaction (R-7). The CO_2 will then react with the SGS in water to form carbamate, which rapidly undergoes hydrolysis to produce glycine and bicarbonate ions according to reaction (R-8) [56]. The CO_2 will also react with H_2O to produce bicarbonate and carbonate ions as expressed above is reactions (R-2) and (R-3), respectively. It should be noted that (R-6) and (R-7) are equilibrium reactions and their corresponding equilibrium constants can be obtained using the change of the standard Gibbs free energy (ΔG°), however, (R-8) is a kinetic reaction whose forward and backward rate constants are required.

$$NH_2CH_2COOH \rightleftharpoons NH_3^+CH_2COO^- \qquad (R-6)$$

$$NH_3^+CH_2COO^- + OH^- \rightleftharpoons NH_2CH_2COO^- + H_2O$$
$$\Delta G^o = -24.17 kJ/mol, \quad \Delta H^o = -11.63 kJ/mol \qquad (R-7)$$

$$NH_2CH_2COO^- + CO_2 + H_2O \underset{k_{1,b}}{\overset{k_{1,f}}{\longleftrightarrow}} NH_3^+CH_2COO^- + HCO_3^- \qquad (R-8)$$

The forward rate constant ($k_{1,f}$) for reaction (R-8) can be calculated by Equation (1) proposed by Lee, Song [72]. Also, based on the standard Gibbs free energy change (ΔG°) and the equilibrium rate constant by Ziemer, Niederhauser [73], we propose Equation (2) to calculate the backward rate constant ($k_{1,b}$) for reaction (R-8). Both $k_{1,f}$ and $k_{1,b}$ are in $m^3/kmol \cdot s$.

$$k_{1,f} = 1.95 \times 10^{13} \exp\left(\frac{-7{,}670}{T}\right) \qquad (1)$$

$$k_{1,b} = 3.82 \times 10^{12} \exp\left(\frac{-9{,}508}{T}\right) \qquad (2)$$

2.4 Washing Unit (WU) for Total SO_2 Removal from the Raw Flue Gas Stream

Since the raw flue gas stream from the power plant contains SO_2 as given in Table 2, a WU was designed to capture all SO_2 from the raw flue gas stream using DIW to produce a desulfurized (sulfur-free) flue gas stream ready for CO_2 capture. The WU is a counter-current fixed-bed absorber packed with Mellapak 250Y. The flow rate of the split raw flue gas (12.43 kg/s) used in our process enters the bottom of the WU at 353.15 K and 1.10 bar and the DIW stream (23.75 kg/s) enters from the top of the WU at 313.15 K and 1.03 bar. A compressor is used to deliver the raw flue gas to the WU at certain superficial gas velocity to overcome the expected pressure drop associated with the resulting counter-current two-phase flow in the unit (fixed-bed reactor).

Following the reaction between SO_2 and DIW as discussed above, the liquid-phase stream coming from the bottom of the WU is sent to a Reverse Osmosis Unit (ROU) for removing the dissolved sulfate ions (SO_4^{2-}) from the "used" DIW. The ROU consists of 60 BW30-400 reverse osmosis membranes [74] arranged in three sets of 30, 18, and 12 membranes, respectively. The permeate (cleaned DIW) from the ROU is then recycled back to the top of the WU for another cycle of SO_2 removal, while the reject from the ROU containing H_2SO_4, can be concentrated and used as an acid, or neutralized using KOH to produce K_2SO_4, which can be used as a fertilizer [75]. On the other hand, the desulfurized flue gas stream coming from the top of the WU is sent directly to the CO_2 CAU, which is also a fixed-bed packed with (Mellapak 250Y) to react with the aqueous SGS stream coming from the top of the CAU. In this study using Aspen Plus v.10, the WU was modelled as a rate-based model, and the ROU with its specifications [76] was represented by one separator. It should be emphasized that there will be no need for this WU, if the raw flue gas is completely sulfur-free, however, in this study, the WU is an integral part of the CO_2 capture process whether in Pathway (i) or Pathway (ii).

2.5 Process Flow Diagram (PFD) for Pathway (i)

Figure 2 shows the PFD for Pathway (i), which also includes the WU. This Pathway is designated to capture at least 90 mol% of CO_2 in the split flue gas stream and preparation it for subsequent sequestration. In this figure, the solution stream coming from the bottom of the CAU is sent to a decanter in which, it exhibits a phase-separation into two phases (CO_2-rich and CO_2-lean). In this Pathway, only the CO_2-rich phase is sent to the stripper for regeneration. It should be noted that the pure CO_2 stream leaving the separator in Figure 2 is further compressed to 152.7 bar using a 2-stage compressor with intercooling. As a result, the water content in this CO_2 stream was only 470 ppm, which is much lower than the limit of 600 ppm maximum set by one of the constraints imposed the process. Thus, this CO_2 stream is ready for subsequent sequestration. It should be noted that like the WU, the CAU was modelled in Aspen Plus v.10 using the rate-based model.

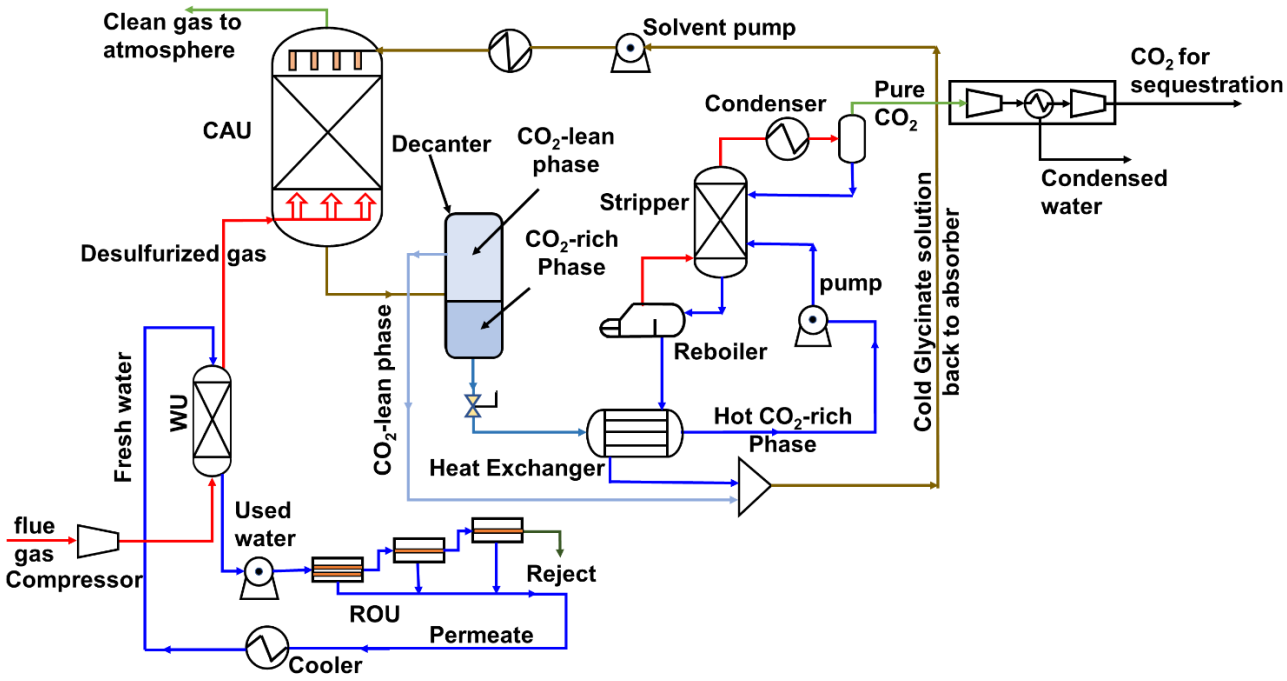

Figure 2 Process flow diagram for pathway (i).

2.6 Process Flow Diagram (PFD) for Pathway (ii)

Figure 3 shows the PFD for Pathway (ii), including the WU, which was discussed above. This Pathway is allotted to CO_2 capture for the production of $NaHCO_3$ nanomaterials. As can be seen in this figure, following the reactions between CO_2 and SGS in the CAU, the resulting solution stream coming from the bottom of the CAU is directly pumped into an Ultra Filtration Unit (UFU), which uses 49 SFP-2880 ultrafiltration membranes by DOW [77]. These membranes are arranged in series and used to separate the nanomaterials from the liquid-phase. In Aspen Plus simulator, like the ROU, the UFU with its specifications [77] was represented by one separator.

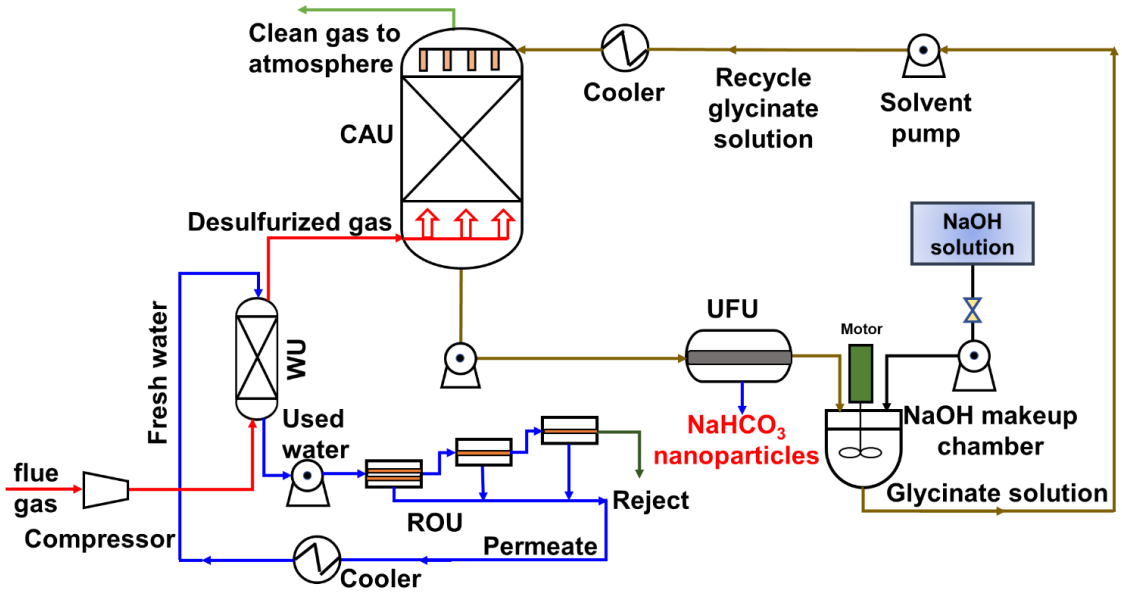

Figure 3 Process flow diagram for pathway (ii).

The filtrate from the UFU containing no nanomaterials is then mixed with NaOH in the makeup chamber, which is a continuously stirred tank reactor (CSTR) used to convert the glycine to SGS. The rection between glycine and NaOH in the CSTR increased the temperature of the SGS produced to a maximum of 338.7 K. This SGS solution is then cooled to 298.15 K and recycled back to the CAU for another cycle of CO_2 capture. It should be underlined that maintaining the temperatures of the inlet DIW to the WU and the inlet SGS to the CO_2 absorber at 298.15 K, lowered the temperature throughout the process including the temperature of the SGS solution produced in the CSTR. This is important for our process since the thermal degradation temperature of SGS reported in the literature was 398 K [78, 79]. It is important to note that sodium glycinate solutions are stable at 220°C [78]. Also, the volatilities of the sodium glycinate solutions (SGS) were reported to be very low [80], resulting in a negligible solvent loss in our process.

3. Design Criteria of Countercurrent Packed-Beds Used in Aspen Plus v.10

As stated above a counter-current packed-bed contactor is suitable for dealing with high flue gas and solvent flow rates due to their high voidage. A packed-bed absorber frequently used in CO_2 capture processes is a cylinder filled with packings of various types, shapes, and sizes whose main function is to increase the turbulence and to spread the liquid over their surfaces thereby increasing the contact area between the gas and liquid phases, which ultimately increases the gas-liquid mass transfer. The packing types are in general random or structured [81]. For using Aspen Plus in our process simulation in a counter-current packed-bed, a precise knowledge of the hydraulics (two-phase pressure drop, liquid holdup, and bed flooding) and mass transfer characteristics (Gas-side (k_G) and liquid-side (k_L) mass transfer coefficients, and specific packing wetted surface area (a_w)) for the gas-liquid systems used is required [82]. Extensive research was conducted to obtain the required available literature correlations for the hydraulics and mass transfer of the gas-liquid systems used in this study. These correlations are discussed in the following.

3.1 Hydraulics Literature Correlations in Counter-Current Packed-Beds

Literature correlations on two-phase pressure drop in packed-beds are mostly empirical and were primarily developed for an air-water system. Sticlmair's [83] and Billet and Schultes' correlations [84] can directly predict the irrigated two-phase pressure drop based on the packing properties, as well as density, viscosity and flow rates of the gas and liquid systems used. Leva's [85] and Kister's [86] correlations, however, need interpolation for pressure drop on pressure drop charts. The literature correlations for the liquid holdup (β_L), representing the liquid retained in the packed-bed during the two-phase flow are usually a function of liquid velocity, liquid density and viscosity, and packing properties [83]. Also, flooding in counter-current packed-beds can be detected using Leva's correlation [85].

3.2 Gas-Liquid Mass Transfer Literature Correlations in Counter-Current Packed-Beds

Onda, Takeuchi [87], Bravo and Fair [88], and Billet and Schultes [89] developed empirical correlations to predict k_L, k_G and a_w, for the gas-liquid systems used in this study using structured packing. These correlations covered wide ranges of gases and solvents with different physico-chemical properties, and the experiments used to develop them were carried under ambient

pressure and temperature, which make them valid for post-combustion CO_2 absorption at ambient conditions.

4. Process Techno-Economic Analysis (TEA)

The TEA calculations include the capital expenditure (CAPEX), operating expenditure (OPEX) and the levelized cost of CO_2 capture (LCOC). The equations used for calculating the total CAPEX of our process equipment can be found elsewhere [90-92]. The installation factors for the equipment used is available in Towler and Sinnott [91]. Also, the Chemical Engineering Plant Cost Index (CEPI) by Lozowski [93] was used to adjust the capital cost to the 2020 USD. The plant was assumed to operate only for 300 days per year. Since LCOC is dependent on the capital and operating costs, the TEA assumptions were, the Plant lifetime (*N*), Annual discount rate (*i*), Capacity factor (f_C), Operating and Maintenance (O&M) cost factor ($f_{O\&M}$) and the Capital recovery factor (f_{CR}). The annual Operating and Maintenance (O&M) cost was assumed to be 4% of total CAPEX as reported in the literature [94, 95] and given in Equations (3) and (4). The recovery factor and the Levelized Cost of CO_2 capture (LCOC) were calculated using Equations (5) and (6), respectively.

$$\mathrm{CAPEX}_{2020} = \sum_{i}^{items} (CAPEX)_{2020,i} \tag{3}$$

$$\mathrm{OPEX}_{2020} = (37 \sum \mathrm{W}) + (\mathrm{C_{NaOH}} \dot{m}_{NaOH} - C_{NaHCO_3} \dot{m}_{NaHCO_3}) + 0.04(\mathrm{CAPEX}_{2020})/7200 \tag{4}$$

$$f_{CR} = \frac{i(1+i)^N}{(1+i)^N - 1} \tag{5}$$

$$\mathrm{LCOC} = \left(\frac{f_{CR}}{f_c}\right) \sum (CAPEX_{2020})/\dot{m}_{CO_2} + OPEX_{2020}/\dot{m}_{CO_2} \tag{6}$$

In this study, the assumed values of these parameters are given in Table 4.

Table 4 Parameters used for LCOC calculation.

Parameter	Value
Cost of electricity [96]	\$37/MWh
i	10%/year
N	30 years
fc	0.8
$f_{O\&M}$	4% of the Total CAPEX, \$/year
f_{CR}	0.10608
C_{NaOH}	Cost of NaOH, 450 \$/ton
$\dot{m}_{NaOH}$	NaOH mass flow rate, ton/h
C_{NaHCO_3}	Cost of $NaHCO_3$, 200 \$/ton
$\dot{m}_{NaHCO_3}$	$NaHCO_3$ mass flow rate, ton/h

5. Results and Discussion

The discussion will follow this sequence: (1) WU and ROU; (2) CO_2 absorber for Pathways (i) and (ii); (3) the stripper in Pathway (i) and the UFU in Pathway (ii); and (4) Comparative TEA for the two Pathways.

5.1 Characteristics of the WU and ROU

The characteristics of the WU and the ROU are given in Table 5 with packing height to absorber internal diameter ratio (H/D) of 6. Table 6 gives the two inlet steams to and two exit steams from the WU. As can be noted, the inlet raw flue gas flow rate is 12.43 kg/s at (at 353.15 K and 1.104 bar), the inlet DIW flow rate is 23.75 kg/s (at 313.15 K and 1.034 bar), the outlet desulfurized flue gas flow rate is 12.10 kg/s (at 314.94 K and 1.034 bar), and the outlet DIW flow rate is 24.08 kg/s (at 326.1 K and 1.03 bar). The ROU consists of three stages, including 60 membranes (type BW30-400 by DOW [74]). The inlet used DIW flow rate to the ROU is 24.08 kg/s at (at 326.1 K and 1.03 bar), the permeate (clean DIW) flow rate is 24.75 kg/s (at 326.1 K and 14.5 bar), and the reject flow rate is 0.33 kg/s (at 326.1 K and 14.5 bar). The permeate is recycled back to the WU.

Table 5 Characteristics of the WU and the ROU.

Inlet DIW flow, kg/s	23.75
Column diameter, m	2.12
Column height, m	15.23
Packing height, m	12.72
Packing type	Mellapak 250Y
ROU membrane type	BW30-400 membrane
Number of membranes	60
Inlet DIW flow, kg/s	23.75

Table 6 Inlet and outlet streams of the WU.

	Inlet flue gas	**Desulfurized flue gas**	**Inlet DIW**	**Outlet DIW**
Pressure, bar	1.104	1.034	1.034	1.031
Temperature, K	353.15	314.94	313.15	326.1
Mass flow rate, kg/s	12.43	12.10	23.75	24.08

5.1.1 Hydraulics and Mass Transfer in the WU

The two-phase pressure, liquid holdup, liquid-side and gas-side mass transfer coefficients, and the normalized specific packing wetted surface area are presented in Figure 4. As can be observed in this figure, the total pressure drop throughout the WU is only 0.08 bar (8 kPa), and there is a strong similarity between the liquid holdup and the normalized specific wetted surface area profiles. Also, the resistance to gas-liquid mass transfer is located in the liquid-side because the liquid-side resistance ($1/k_L$) is greater than gas-side resistance ($1/k_G$).

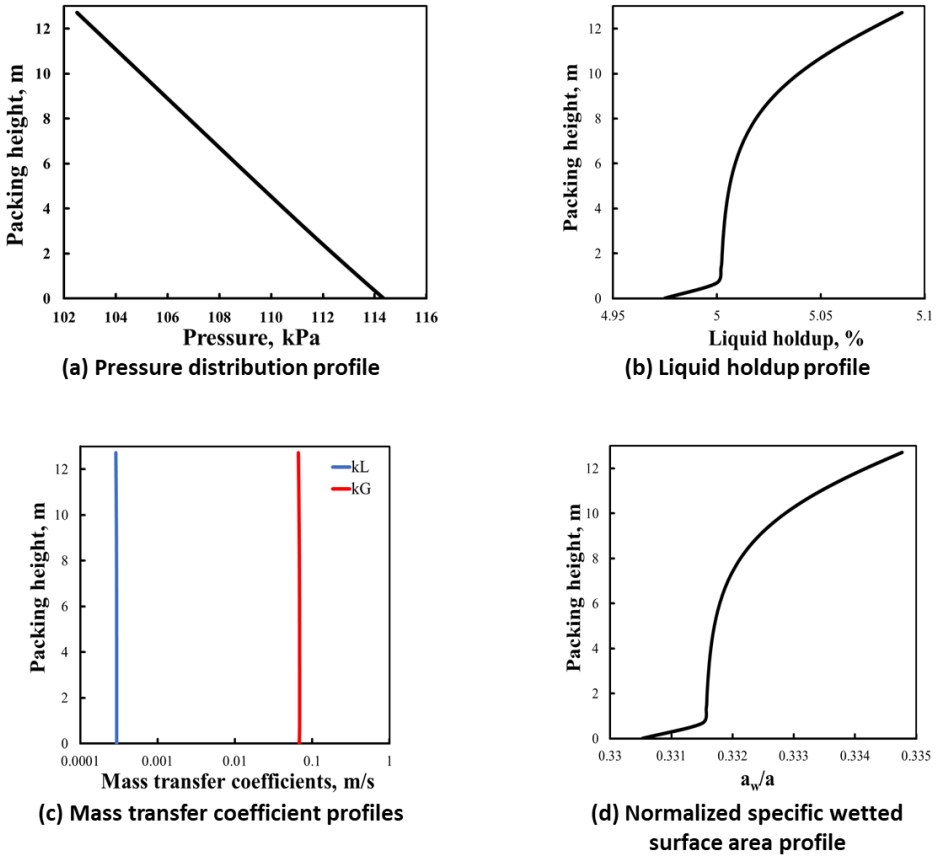

Figure 4 Hydraulics and mass transfer in the WU.

5.1.2 Performance of the WU and ROU

The performance of the WU in term of the composition of each component in the inlet and outlet streams of the WU is given in Table 7. As can be observed the desulfurized flue gas is completely sulfur-free, and the CO_2 content of this stream going to the absorber is 20.7 wt%.

Table 7 Performance of the WU.

	Inlet flue gas	**Desulfurized flue gas**	**Inlet DIW**	**Outlet DIW**
Components	wt%	wt%	wt%	wt%
CO_2	20.18	20.71	5.34×10^{-4}	1.05×10^{-2}
H_2O	7.63	5.13	99.99	99.98
N_2	67.79	69.64	4.93×10^{-5}	9.73×10^{-4}
O_2	4.4	4.52	5.87×10^{-6}	1.16×10^{-4}
SO_2	0.0052	0	0	0
H_2SO_4	0	0	2.18×10^{-4}	4.29×10^{-3}

The SO_2 absorption efficiency profile is shown in Figure 5, and as can be seen the WU is able to completely remove SO_2 from the flue gas split stream. Actually, a packing height of about 6.0 m is largely sufficient for the removal of 100 mol% of SO_2 from the split flue gas stream rather than 12.72 m. However, the packing height to internal diameter ratio (H/D) of a fixed-bed reactor was

constrained in this study to be greater than 6 to avoid fluid channeling. Therefore, the packing height of the WU was calculated as 12.72 m.

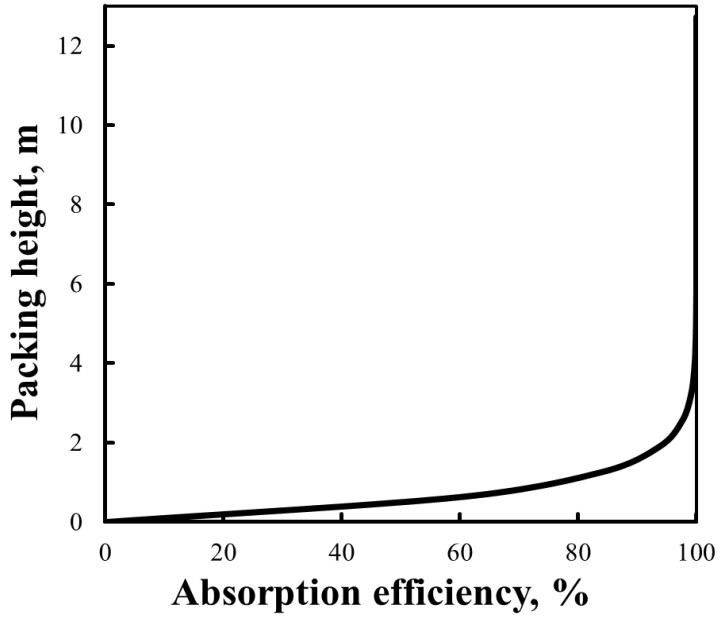

Figure 5 SO_2 absorption efficiency profile in the WU.

Also, considering the flow rates of the used DIW and the permeate, the performance of the ROU in removing the dissolved SO_2 from the used DIW stream is almost 100 wt%.

5.1.3 Characteristics of the CAU in the Two Pathways

Table 8 shows the characteristics of the CAU used for Pathways (i) and (ii); and as can be observed more solvent flow rate and taller absorber are used in Pathway (i) than Pathway (ii) to have the same absorption efficiency. It is important to note that the flow rates of 53 L/s and 30 L/s are the minimum solvents flow rates of Pathways (i) and (ii) to meet the CAU absorption efficiency, which was constrained to at least 90 mol% CO_2 capture from the flue gas stream. The residence time of the desulfurized flue gas in the CAU was 137.1 s for pathway (i) and 104.1 s for pathway (ii). These residence times in the CAU lie within the reported residence time ranges (10-200 s) for post-combustion CO_2 absorption using ethanolamines in packed-beds [97, 98]. These residence times for SGS are longer than those in ethanolamines since the reaction kinetics of CO_2 and SGS are slower when compared with those of CO_2 and ethanolamines.

Table 8 Characteristics of the CAU in the two pathways.

	Pathway (i)	**Pathway (ii)**
Pressure, bar	1.013	1.013
Temperature, K	313.15	298.15
Mass flow rate of 3M SGS solution, kg/s	58	33
Solvent flow rate, L/s	53	30
Column diameter, m	6	6
Column height, m	63.42	39.42

Packing height, m	60	36
CO_2 capture efficiency, mol%	91	91
Packing type	Mellapak 250Y	

5.1.4 Hydraulics and Mass Transfer in the CAU

Table 9 shows that the absorber hydraulics and mass transfer characteristics in Pathways (i) and (ii), expressed in terms of pressure drop, liquid holdup, and normalized specific packing wetted surface area, are nearly the same. The hydraulics and mass transfer were sensitive to the solvent flow rate, and physico-chemical properties of the liquid and gas phases. Faster the solvent flow rate, higher the liquid hold-up, and larger the mass transfer coefficients and the normalized specific packing wetted area.

Table 9 Hydraulics and mass transfer in the CAU.

	Pathway (i)	**Pathway (ii)**
Pressure drop, bar	0.006	0.004
Liquid holdup, vol%	5.17-5.50	4.27-4.83
Normalized specific packing wetted area, -	0.243-0.246	0.193-0.200
Liquid-side mass transfer coefficients (k_L), m/s	1.61×10^{-4}-2.26×10^{-4}	8.22×10^{-5}-1.21×10^{-4}
Gas-side mass transfer coefficient (k_G), m/s	2.49×10^{-2}-2.83×10^{-2}	1.25×10^{-2}-1.69×10^{-2}
Packing type	Mellapak 250Y	

5.1.5 Performance of the CAU in Pathways (i) and (ii)

Considering the characteristics of the CAU given in Table 8, the CO_2 removal efficiency in Pathway (i) is 91 mol%, which is very close to that (90.7 mol%) in Pathway (ii) even though the solvent flow rate and packing height in Pathway (i) are respectively 77% and 67% greater than those in Pathway (ii). This behavior can be related to the composition of the recycled solvent in the case of Pathway (i). Different from Pathway (ii), the recycled liquid solvent in Pathway (i) is not 100% SGS, which appeared to dramatically affect the SGS chemical reaction kinetics with CO_2 in the flue gas stream. Actually, only 62 mol% of $NaHCO_3$ is in CO_2-rich phase, which is sent to the stripper for regeneration and further recycling to the absorber.

In Pathway (i), the CO_2-rich stream coming from the absorber is sent directly to decanter, in which the solution exhibits a phase separation into CO_2-rich and CO_2-lean phases. The CO_2-rich phase represents 25 vol% of the solution and contains 62 mol% of $NaHCO_3$ nanomaterials. In this study, only the CO_2-rich phase is sent for regeneration in a stripper. The characteristics of the stripper used in Pathway (i) are given in Table 10.

Table 10 Characteristics of the stripper used in Pathway (i).

Stripper diameter, m	3
Stripper height, m	20.78
Packing height, m	18
Packing type	Mellapak 250Y

Reboiler duty, MW	4.04
Reboiler temperature, K	396.21
Condenser duty, MW	-0.82
Condenser temperature, K	293.15

In Pathway (ii), the liquid stream coming from the absorber (CAU) is sent directly to the UFU, which uses 49 SFP-2880 ultrafiltration membrane by DOW [77] to separate the $NaHCO_3$ nanomaterials. The separation efficiency of this membrane was estimated at 99.95%. Ultimately, the production of 15.62 ton/h of $NaHCO_3$ nanomaterials in Pathway (ii) requires the use of SFP-2880 ultrafiltration membrane in the UFU and an NaOH make-up rate of 7.43 ton/h. It should be noted that the CO_2 released upon regeneration is sent to a two-stage compressor to boost its pressure to 152.7 bar, which makes it ready for subsequent sequestration.

The mass flow rate and composition of the stream in the decanter and stripper are given in Table 11. At steady state, the total flow rate of the water and $NaHCO_3$ in the solution coming from bottom of the CAU were 150.7 ton/h, and 25.3 ton/h, respectively. Due to phase separation, the water and $NaHCO_3$ flow rates in the upper phase were 113.0 ton/h and 9.6 ton/h, while the water and $NaHCO_3$ flow rates in the lower phase were 37.7 ton/h and 15.7 ton/h, respectively. This means that the amount of water in the lower phase represents only 25 wt% of the total water in the solution. In pathway (i), only the lower phase was sent to the stripper for regeneration and since the amount of water in this stream was small, the stripper reboiler duty required to remove all CO_2 from this phase was only 4.04 MW. The regenerated stream from the reboiler (44.6 ton/h) consisted of 16.73 wt% NaOH, and 83.27 wt% H_2O. Also, in pathway (i), the upper phase (171.6 ton/h) composed of 15.36 wt% SGS, 13.16 wt% glycine, and 5.6 wt% of $NaHCO_3$ and 65.88 wt% H_2O. This upper phase was not regenerated, rather it was mixed with regenerated stream from the reboiler and recycled back to the CAU. Upon the reaction between NaOH and glycine, the recycled stream to the CAU consisted of 20.42 wt% SGS, 4.08 wt% Glycine, 4.5 wt % $NaHCO_3$, and 71.0 wt% H_2O. Thus, the recycled liquid stream to the CAU was not pure SGS solution.

Table 11 Decanter and stripper stream results.

	CO_2-rich out (CAU)	**Upper phase (decanter)**	**Bottom-phase (decanter)**	**CO_2-Lean out (stripper)**	**Recycled to (CAU)**
Mass flow rate, ton/h	224.96	171.60	53.36	44.59	216.19
			Mass percentage (wt%)		
SGS	11.72	15.36	-	-	20.42
H_2O	67.01	65.88	70.63	83.27	71.00
Glycine	10.04	13.16	-	-	4.08
$NaHCO_3$	11.23	5.60	29.47	-	4.50
NaOH	-	-	-	16.73	-
CO_2	-	-	-	-	-

5.2 CAPEX and OPEX of Pathways (i) and (ii)

Table 12 shows the calculated CAPEX ($12,039,251) and OPEX (261 $/h) of Pathways (i) are much greater than the CAPEX ($5,908,000) and OPEX (237.24 $/h) for Pathway (ii). This behavior could be attributed to the cost of the stripper, initial solvent cost, heat exchangers, rotating equipment, as well as a more expensive larger CO_2 absorber in Pathway (i).

Table 12 CAPEX and OPEX of Pathways (i) and (ii).

	Pathway (i)	**Pathway (ii)**
CAPEX, USD 2020		
Heat Exchangers	$5,501,400	$1,872,719
Packing Cost	$324,618	$181,182
Absorber	$2,886,734	$2,319,957
Initial solvent cost	$862,826	$202,437
Washing unit	$253,682	$253,682
Rotating equipment	$1,481,531	$349,999
ROU	$153,250	$153,250
UFU	--	$127,020
Reaction Chamber	--	$447,755
Stripper	$575,211	--
Total CAPEX, 2020 USD	**$12,039,251**	**$5,908,000**
OPEX, USD 2020/h		
NaOH makeup	--	3,345,7
$NaHCO_3$ production	--	-3,169.9
O&M	66.88	32.82
Total electricity cost	194.23	28.71
Total OPEX, 2020 USD/h	**261.11**	**237.24**

Table 13 gives the LCOC values for both Pathways, and as can be seen, the LCOC (54.01 2020-USD/ton-CO_2 captured) of Pathway (i) is greater than the LCOC (39.90 2020-USD/ton-CO_2 captured) of Pathway (ii). This is not surprising considering the higher CAPEX and OPEX associated with Pathway (i) than Pathway (ii).

In addition, Pathway (ii) can capture 8.19 ton/h of CO_2 and produce 15.62 ton/h of saleable $NaHCO_3$ solid nanomaterials, and Pathway (i) can capture 8.21 ton/h of CO_2 with 99.95 mol% purity, which can be used or sent for sequestration.

Table 13 LCOC of Pathways (i) and (ii).

	Pathway (i)	**Pathway (ii)**
Capacity factor, f_C	0.8	
Discount rate i, 1/year	10%	
Lifetime N, year	30	
Capital recovery factor f_{CR}, 1/year	0.106079	
$\dot{m}_{CO_2}$, ton/h	8.21	8.16

$NaHCO_3$ produced, ton/h	-	15.62
CAPEX to LCOC, \$/ton-CO_2	22.20	10.92
OPEX to LCOC, \$/ton-CO_2	31.81	28.98
Total LCOC, \$/ton-CO_2	**54.01**	**39.90**

5.3 Sensitivity Analysis for Pathway (ii)

We have conducted sensitivity analysis for pathway (ii). The CAU unit was 6 m diameter packed with Mellapak 250Y to a height of 36 m. The power plant capacity, SGS molarity, and SGS flow rate were varied to study their effects on the TEA (CAPEX, OPEX, and LCOC), hydraulics (two-phase pressure drop and liquid holdup), and the normalized specific wetted area of the packing. These results are given in Table 14, Table 15, and Table 16, where all TEA costs are in 2020-USD. Table 14 shows that increasing the power plant capacity at 3 M (mol/L) of SGS and about 90 mol% CO_2 capture, increases the CAPEX, OPEX and liquid holdup, CAU pressure drop and normalized packing specific wetted area, but decreases the LCOC of the process. These data are in agreement with previous finding for pre-combustion CO_2 capture applications presented by [92], Ashkanani, Wang [94]. Table 15 shows that increasing the SGS molarity in mol/L increases the CO_2 capture efficiency, CAPEX, OPEX, liquid holdup, and normalized packing specific wetted area, but decreases the LCOC of the process. Table 16 shows that increasing the SGS flow rate in L/s increases the CO_2 capture efficiency, CAPEX, OPEX, liquid holdup, and the normalized packing specific wetted area, but decreases the LCOC of the process.

Table 14 Effect of power plant capacity on the process TEA, hydraulics, and the normalized packing specific wetted area (SGS = 3M).

Plant Capacity (MWe)	**CO_2 absorption efficiency (%)**	**CAPEX (Million USD)**	**OPEX (USD/h)**	**LCOC (USD/ton.CO_2)**	**Liquid holdup (%)**	**CAU pressure drop (Pa)**	**a_w/a (%)**
6	90.29	5.01	75.83	46.03	3.61-4.04	161	15.7-16.2
10	90.73	5.91	89.40	39.90	4.27-4.83	396	19.3-20.0
30	90.08	9.51	143.93	33.61	6.10-7.04	2,989	30.0-31.1
60	90.07	14.45	218.69	32.06	7.01-8.18	7,568	35.6-37.1
120	90.86	23.99	363.07	31.66	7.66-8.85	16,079	39.5-41.1

Table 15 Effect of SGS molarity on the process CO_2 absorption efficiency, TEA, hydraulics and the normalized packing specific wetted area.

SGS molarity, (mol/L)	CO_2 absorption efficiency (%)	CAPEX (Million USD)	OPEX (USD/h)	LCOC USD/ton.CO_2	Liquid Holdup (%)	CAU pressure drop, (Pa)	a_w/a (%)
1.0	44.38	5.72	86.51	55.88	4.09-4.26	353	17.1-17.34
1.5	59.89	5.80	87.74	47.87	4.11-4.36	362	17.5-17.9
2.0	72.18	5.84	88.47	44.01	4.15-4.49	372	18.1-18.5
2.5	82.22	5.88	89.04	41.51	4.21-4.65	384	18.6-19.2
3.0	90.73	5.91	89.40	39.90	4.27-4.83	396	19.3-20.0
3.5	97.99	5.92	89.55	38.70	4.37-5.05	407	20.0-20.8

Table 16 Effect of SGS solvent flow rate on the process CO_2 absorption efficiency, TEA, hydraulics, and the normalized packing specific wetted area (SGS = 3 M).

SGS flow rate (L/s)	CO_2 absorption efficiency (%)	CAPEX (Million USD)	OPEX (USD/h)	LCOC (USD/ton.CO_2)	Liquid holdup (%)	CAU pressure drop (Pa)	a_w/a (%)
20	63.65	5.60	84.76	45.28	3.86-4.31	387.85	16.5-17.2
22	69.30	5.66	85.72	43.78	3.96-4.41	389.84	17.1-17.8
24	74.83	5.72	86.65	42.54	4.05-4.50	391.76	17.7-18.3
26	80.26	5.79	87.57	41.50	4.13-4.58	393.51	18.3-18.9
28	85.56	5.85	88.50	40.63	4.20-4.66	394.98	18.8-19.4
30	90.73	5.91	89.40	39.90	4.27-4.83	395.91	19.3-20.0

6. Concluding Remarks

In this study, a unique process using aqueous SGS for CO_2 capture from a split stream of actual flue gas containing 0.0023 mol% SO_2 and 13.33 mol% CO_2 was developed in Aspen Plus v.10. The flow rate of the split stream used was maintained at 12.43 kg/s and the SGS flow rate was varied to

capture more than 90 mol% CO_2 from the split flue gas stream. The process has two Pathways (i) to capture and prepare CO_2 for sequestration and (ii) to produce $NaHCO_3$ nanomaterials. Since the raw flue gas contained SO_2, a WU was designed to remove all SO_2 before CO_2 capture in both Pathways.

The physico-chemical properties of the aqueous SGS solutions were obtained from the literature, regressed, and implemented in Aspen Plus v.10. The CO_2-SGS reaction kinetics were also obtained and the system hydraulics (two-phase pressure drop and liquid holdup), and mass transfer characteristics (gas-side and liquid-side mass transfer coefficients and the normalized specific wetted surface area of the packing) were calculated. The total CAPEX, OPEX, and LCOC of the two Pathways were also calculated. The WU and CAU are counter-current fixed-bed absorbers packed with Mellapak 250Y.

Under the operating conditions used, no flooding was observed in WU and CAU. The two-phase pressure, liquid holdup, liquid-side and gas-side mass transfer coefficients and the normalized specific wetted area of packing in the WU and CAU were obtained and presented as a function of the packing height. The data in both units indicated that the gas-side mass transfer coefficients were much greater than the liquid-side mass transfer coefficients and the behavior of the liquid holdup and the normalized specific wetted area of packing were similar in both units. Our hydraulics predictions, however, need to be validated against actual data from an industrial post-combustion power plant.

Aspen Plus TEA calculations showed that considering a plant lifetime of 30 years, an annual discount rate of 10%, a capacity factor of 0.8, an annual O&M cost factor of 4% of the total CAPEX in 2020-USD, and a capital recovery factor of 0.106, the CAPEX, OPEX and LCOC of the Pathway (i) were ($12,039,251), (261 $/h), and (54.01 $/ton of CO_2 captured), respectively. Also, the CAPEX, OPEX and LCOC of the Pathway (ii) were ($5,908,000), (237 $/h), and (39.90 $/ton of CO_2 captured), respectively. In addition, Pathway (i) can capture 8.21 ton/h of CO_2 with 99.95 mol% purity, which are ready for subsequent sequestration, however, Pathway (ii) can capture 8.16 ton/h of CO_2 and produce 15.62 ton/h of saleable $NaHCO_3$ solid nanomaterials.

7. Future Prospects and Challenges

Among the 20 known amino acids, Gly and Alanine (ALA) react with CO_2 to produce nanomaterials, which exhibit a phase separation (CO_2-rich and CO_2-lean phases) and subsequently there are potential opportunities for using aqueous amino acid salts for CO_2 capture and producing high-value nanomaterials, which can be sold to offset the overall cost of the capture process. The selection of the base (NaOH, KOH, etc.) to react with the amino acid could open more venues in CO_2 capture, while producing vital products with many diverse applications. For instance, sodium bicarbonate could be used in baking and personal hygiene, as food additives, a disinfectant, a fire extinguisher, and as a promising agent for cancer therapy [3]. Also, the potassium bicarbonate could be used for food and drink, fire extinguisher, and agriculture, especially for acidic soil neutralization and organic farming [99, 100]. The choice of the base could also enhance its reaction kinetics with CO_2 so that amino acid salts could be used to capture small concentrations of CO_2 whether from Natural Gas Combined Cycles (NGCC) or direct air capture (DAC). The challenges in using amino acid salts for CO_2 capture reside in maintaining bicarbonates in the presence of side-products and separating the nanomaterials from the liquor in a continuous process. Also, the availability of ample capacity of NaOH could be a challenge, however, our estimates showed that NaOH available in the

market was more than enough for our process. Another challenge is the ability of amino acids to achieve a net negative CO_2 emission, which could be assessed by performing Life Cycle Analysis (LCA) along with the TEA of the process.

Acknowledgement

The manuscript is based upon work supported by the Department of Energy under Award Number (DE-FE0031707).

Author Contributions

Mr. Rui Wang collected the data and performed the TEA; and Drs. Husain Ashkanani, Bingyun Li, and Badie Morsi revised and polished the manuscript.

Competing Interests

This manuscript was prepared as an account of work sponsored by an agency of the United States Government. Neither the United States Government nor any agency thereof, nor any of their employees, makes any warranty, express or implied, or assumes any legal liability or responsibility for the accuracy, completeness, or usefulness of any information, apparatus, product, or process disclosed, or represents that its use would not infringe privately owned rights. Reference herein to any specific commercial product, process, or service by trade name, trademark, manufacturer, or otherwise does not necessarily constitute or imply its endorsement, recommendation, or favoring by the United States Government or any agency thereof. The views and opinions of authors expressed herein do not necessarily state or reflect those of the United States Government or any agency thereof.

References

1. Kweku DW, Bismark O, Maxwell A, Desmond KA, Danso KB, Oti-Mensah EA, et al. Greenhouse effect: Greenhouse gases and their impact on global warming. J Sci Res Rep. 2018; 17: 1-9.
2. Zhongming Z, Linong L, Xiaona Y, Wangqiang Z, Wei L. Choices made now are critical for the future of our ocean and cryosphere [Internet]. Geneva: IPCC; 2019. Available from: https://www.ipcc.ch/2019/09/25/srocc-press-release/.
3. Sun J, Chow AC, Madanat SM. Equity concerns in transportation infrastructure protection against sea level rise. Transp Policy. 2021; 100: 81-88.
4. Galbraith SM, Cane JH, Rivers JW. Wildfire severity influences offspring sex ratio in a native solitary bee. Oecologia. 2021; 195: 65-75.
5. Nagelkerken I, Alemany T, Anquetin JM, Ferreira CM, Ludwig KE, Sasaki M, et al. Ocean acidification boosts reproduction in fish via indirect effects. PLOS Biol. 2021; 19: e3001033.
6. Rayer Q, Pfleiderer P, Haustein K. Global warming and extreme weather investment risks. In: Ecological, societal, and technological risks and the financial sector. Cham: Springer; 2020. pp. 39-68.
7. CO_2 emissions [Internet]. London: BP; Available from: https://www.bp.com/en/global/corporate/energy-economics/statistical-review-of-world-energy/co2-emissions.html.

8. CO_2 emissions from fuel combustion-2020 edition [Internet]. Paris: IEA; 2020. Available from: https://iea.blob.core.windows.net/assets/474cf91a-636b-4fde-b416-56064e0c7042/WorldCO2_Documentation.pdf.
9. Global CO_2 emissions by sector, 2019 [Internet]. Paris: IEA; 2021. Available from: https://www.iea.org/data-and-statistics/charts/global-co2-emissions-by-sector-2019.
10. van Vuuren DP, Stehfest E, Gernaat DEHJ, van den Berg M, Bijl DL, de Boer HS, et al. Alternative pathways to the 1.5 °C target reduce the need for negative emission technologies. Nat Clim Chang. 2018; 8: 391-397.
11. Report of the Conference of the Parties on its twenty-first session, held in Paris from 30 November to 13 December 2015. Addendum. Part two: Action taken by the Conference of the Parties at its twenty-first session. Bonn: UNFCCC Secretariat; 2016. FCCC/CP/2015/10/Add.1.
12. Rogelj J, Shindell D, Jiang K, Fifita S, Forster P, Ginzburg V, et al. Mitigation pathways compatible with 1.5°C in the context of sustainable development. In: Global warming of 15°C. Geneva: Intergovernmental Panel on Climate Change; 2018. pp. 93-174.
13. Tzimas V. 2011 technology map of the European strategic energy technology plan (SET-Plan). Technology descriptions. Petten: IET; 2011. EUR-24979-EN-2011.
14. Ketzer JM, Iglesias RS, Einloft S. Reducing greenhouse gas emissions with CO_2 capture and geological storage. In: Handbook of climate change mitigation and adaptation. New York: Springer; 2015. pp. 1-40.
15. Electricity information-April 2020 edition [Internet]. Paris: IEA; Available from: https://iea.blob.core.windows.net/assets/e5ee2901-204b-4977-8d6c-91b97e69dd94/Ele_documentation.pdf.
16. Rubin ES, Chen C, Rao AB. Cost and performance of fossil fuel power plants with CO_2 capture and storage. Energy Policy. 2007; 35: 4444-4454.
17. Chao C, Deng Y, Dewil R, Baeyens J, Fan X. Post-combustion carbon capture. Renew Sust Energ Rev. 2021; 138: 110490.
18. Zhao H, Luo X, Zhang H, Sun N, Wei W, Sun Y. Carbon-based adsorbents for post-combustion capture: A review. Greenhouse Gas Sci Technol. 2018; 8: 11-36.
19. Peng Y, Zhao B, Li L. Advance in post-combustion CO_2 capture with alkaline solution: A brief review. Energy Procedia. 2012; 14: 1515-1522.
20. Darde V, Thomsen K, van Well WJM, Stenby EH. Chilled ammonia process for CO_2 capture. Energy Procedia. 2009; 1: 1035-1042.
21. Liu J, Wang S, Zhao B, Tong H, Chen C. Absorption of carbon dioxide in aqueous ammonia. Energy Procedia. 2009; 1: 933-940.
22. Jiang K, Yu H, Yu J, Li K. Advancement of ammonia-based post-combustion CO_2 capture technology: Process modifications. Fuel Process Technol. 2020; 210: 106544.
23. Benson HE, Field JH, Jimeson RM. CO_2 absorption: Employing hot potassium carbonate solutions. Chem Eng Prog. 1954; 50: 356-364.
24. Anderson C, Harkin T, Ho M, Mumford K, Qader A, Stevens G, et al. Developments in the CO2CRC uno MK 3 process: A multi-component solvent process for large scale CO_2 capture. Energy Procedia. 2013; 37: 225-232.
25. Anderson C, Hooper B, Qader A, Harkin T, Smith K, Mumford K, et al. Recent developments in the UNO MK 3 process – A low cost, environmentally benign precipitating process for CO_2 capture. Energy Procedia. 2014; 63: 1773-1780.

26. Smith K, Xiao G, Mumford K, Gouw J, Indrawan I, Thanumurthy N, et al. Demonstration of a concentrated potassium carbonate process for CO_2 capture. Energy Fuels. 2014; 28: 299-306.
27. Rangwala HA, Morrell BR, Mather AE, Otto FD. Absorption of CO_2 into aqueous tertiary amine/mea solutions. Can J Chem Eng. 1992; 70: 482-490.
28. Chakma A, Mehrotra AK, Nielsen B. Comparison of chemical solvents for mitigating CO_2 emissions from coal-fired power plants. Heat Recovery Syst CHP. 1995; 15: 231-240.
29. Versteeg G, Van Dijck L, van Swaaij WPM. On the kinetics between CO_2 and alkanolamines both in aqueous and non-aqueous solutions. An overview. Chem Eng Commun. 1996; 144: 113-158.
30. Saha AK, Bandyopadhyay SS, Biswas AK. Kinetics of absorption of CO_2 into aqueous solutions of 2-amino-2-methyl-1-propanol. Chem Eng Sci. 1995; 50: 3587-3598.
31. Li K, Cousins A, Yu H, Feron P, Tade M, Luo W, et al. Systematic study of aqueous monoethanolamine-based CO_2 capture process: Model development and process improvement. Energy Sci Eng. 2016; 4: 23-39.
32. Oexmann J, Kather A, Linnenberg S, Liebenthal U. Post-combustion CO_2 capture: Chemical absorption processes in coal-fired steam power plants. Greenhouse Gas Sci Technol. 2012; 2: 80-98.
33. Godini HR, Mowla D. Selectivity study of H_2S and CO_2 absorption from gaseous mixtures by mea in packed beds. Chem Eng Res Des. 2008; 86: 401-409.
34. Zhang Y, Chen CC. Thermodynamic modeling for CO_2 absorption in aqueous mdea solution with electrolyte nrtl model. Ind Eng Chem Res. 2011; 50: 163-175.
35. Böttinger W, Maiwald M, Hasse H. Online NMR spectroscopic study of species distribution in MEA–H_2O–CO_2 and DEA–H_2O–CO_2. Fluid Phase Equilib. 2008; 263: 131-143.
36. El Hadri N, Quang DV, Goetheer ELV, Abu Zahra MRM. Aqueous amine solution characterization for post-combustion CO_2 capture process. Appl Energy. 2017; 185: 1433-1449.
37. Versteeg GF, Van Swaaij WPM. Solubility and diffusivity of acid gases (carbon dioxide, nitrous oxide) in aqueous alkanolamine solutions. J Chem Eng Data. 1988; 33: 29-34.
38. Xu S, Otto FD, Mather AE. Physical properties of aqueous amp solutions. J Chem Eng Data. 1991; 36: 71-75.
39. Saha AK, Bandyopadhyay SS, Biswas AK. Solubility and diffusivity of nitrous oxide and carbon dioxide in aqueous solutions of 2-amino-2-methyl-1-propanol. J Chem Eng Data. 1993; 38: 78-82.
40. Aroonwilas A, Tontiwachwuthikul P. High-efficiency structured packing for CO_2 separation using 2-amino-2-methyl-1-propanol (AMP). Sep Purif Technol. 1997; 12: 67-79.
41. Vázquez G, Alvarez E, Navaza JM, Rendo R, Romero E. Surface tension of binary mixtures of water + monoethanolamine and water + 2-amino-2-methyl-1-propanol and tertiary mixtures of these amines with water from 25 °C to 50 °C. J Chem Eng Data. 1997; 42: 57-59.
42. Chen YJ, Li MH. Heat capacity of aqueous mixtures of monoethanolamine with 2-amino-2-methyl-l-propanol. J Chem Eng Data. 2001; 46: 102-106.
43. Ko JJ, Tsai TC, Lin CY, Wang HM, Li MH. Diffusivity of nitrous oxide in aqueous alkanolamine solutions. J Chem Eng Data. 2001; 46: 160-165.
44. Álvarez E, Cancela Á, Maceiras R, Navaza JM, Táboas R. Surface tension of aqueous binary mixtures of 1-amino-2-propanol and 3-amino-1-propanol, and aqueous ternary mixtures of these amines with diethanolamine, triethanolamine, and 2-amino-2-methyl-1-propanol from (298.15 to 323.15) K. J Chem Eng Data. 2003; 48: 32-35.

45. Henni A, Hromek JJ, Tontiwachwuthikul P, Chakma A. Volumetric properties and viscosities for aqueous AMP solutions from 25 °C to 70 °C. J Chem Eng Data. 2003; 48: 551-556.
46. Mandal BP, Kundu M, Bandyopadhyay SS. Physical solubility and diffusivity of N_2O and CO_2 into aqueous solutions of (2-amino-2-methyl-1-propanol + monoethanolamine) and (N-methyldiethanolamine + monoethanolamine). J Chem Eng Data. 2005; 50: 352-358.
47. Arcis H, Rodier L, Coxam JY. Enthalpy of solution of CO_2 in aqueous solutions of 2-amino-2-methyl-1-propanol. J Chem Thermodyn. 2007; 39: 878-887.
48. Chakraborty A, Astarita G, Bischoff K. CO_2 absorption in aqueous solutions of hindered amines. Chem Eng Sci. 1986; 41: 997-1003.
49. Aboudheir A, Tontiwachwuthikul P, Idem R. Rigorous model for predicting the behavior of CO_2 absorption into AMP in packed-bed absorption columns. Ind Eng Chem Res. 2006; 45: 2553-2557.
50. Law LC, Azudin NY, Shukor SRA. Optimization and economic analysis of amine-based acid gas capture unit using monoethanolamine/methyl diethanolamine. Clean Technol Environ Policy. 2018; 20: 451-461.
51. Song HJ, Lee S, Maken S, Park JJ, Park JW. Solubilities of carbon dioxide in aqueous solutions of sodium glycinate. Fluid Phase Equilib. 2006; 246: 1-5.
52. Song HJ, Lee S, Park K, Lee J, Chand Spah D, Park JW, et al. Simplified estimation of regeneration energy of 30 wt% sodium glycinate solution for carbon dioxide absorption. Ind Eng Chem Res. 2008; 47: 9925-9930.
53. Salazar Vn, Sánchez-Vicente Y, Pando C, Renuncio JA, Cabañas A. Enthalpies of absorption of carbon dioxide in aqueous sodium glycinate solutions at temperatures of (313.15 and 323.15) K. J Chem Eng Data. 2009; 55: 1215-1218.
54. Mazinani S, Samsami A, Jahanmiri A, Sardarian A. Solubility (at low partial pressures), density, viscosity, and corrosion rate of carbon dioxide in blend solutions of monoethanolamine (MEA) and sodium glycinate (SG). J Chem Eng Data. 2011; 56: 3163-3168.
55. Lee S, Choi SI, Maken S, Song HJ, Shin HC, Park JW, et al. Physical properties of aqueous sodium glycinate solution as an absorbent for carbon dioxide removal. J Chem Eng Data. 2005; 50: 1773-1776.
56. Park SW, Son YS, Park DW, Oh KJ. Absorption of carbon dioxide into aqueous solution of sodium glycinate. Sep Sci Technol. 2008; 43: 3003-3019.
57. Lee S, Song HJ, Maken S, Yoo SK, Park JW, Kim S, et al. Simulation of CO_2 removal with aqueous sodium glycinate solutions in a pilot plant. Korean J Chem Eng. 2008; 25: 1-6.
58. Vaidya PD, Konduru P, Vaidyanathan M, Kenig EY. Kinetics of carbon dioxide removal by aqueous alkaline amino acid salts. Ind Eng Chem Res. 2010; 49: 11067-11072.
59. Li B, Wang X, Hopkinson D, Hoffman J, Egbebi A, Resnik KP. Amino acids react with carbon dioxide (CO_2) and form nanofibers and nanoflowers. Morgantown: West Virginia University; 2020. US10583388B2.
60. Bennion EB, Bamford GST, Bent AJ. Sugars. In: The technology of cake making. Boston: Springer; 1997. pp. 84-99.
61. Tucker W, Aslam M, Lema M, Shin I, Le Ruyet P, Hogue J, et al. Sodium bicarbonate or multielement buffer via diet or rumen: Effects on performance and acid-base status of lactating cows. J Dairy Sci. 1992; 75: 2409-2420.

62. Domino. How to get rid of bad kitchen smells [Internet]. New York: Tasting Table; 2017. Available from: https://www.tastingtable.com/cook/national/bad-kitchen-smells-odors.
63. Bonfim-Rocha L, Silva AB, de Faria SHB, Vieira MF, de Souza M. Production of sodium bicarbonate from CO_2 reuse processes: A brief review. 2020; 18: 20180318.
64. Hoffman H, Wu S, Pardini R, Tripp E, Barnes D. Expansion of michigan EOR operations using advanced amine technology at a 600 MW project wolverine carbon capture and storage project. Final Report. Cadillac: Wolverine Power Supply Cooperative; 2010. DE-FE000247.
65. Geankoplis CJ. Principles of momentum transfer and applications. In: Transport process and unit operations. Singapore: Prentice-Hall. 1995. pp. 114-213.
66. Pilling M, Holden BS. Choosing trays and packings for distillation. Am Inst Chem Eng CEP. 2009; 105: 44-50.
67. Wu A, Yin S, Yang B, Wang J, Qiu G. Study on preferential flow in dump leaching of low-grade ores. Hydrometallurgy. 2007; 87: 124-132.
68. Cussler EL. Diffusion: Mass transfer in fluid systems. New York: Cambridge university press; 2009.
69. Sander R. Compilation of Henry's law constants (version 4.0) for water as solvent. Atmos Chem Phys. 2015; 15: 4399-4981.
70. Aspen Plus. Rate based model of the CO_2 capture process by MEA using Aspen Plus. Cambridge: Aspen Technology Inc.; 2008.
71. Weiland RH, Hatcher NA, Nava JL. Post-combustion CO_2 capture with amino-acid salts. GPA Eur. 2010; 22: 24.
72. Lee S, Song HJ, Maken S, Park JW. Kinetics of CO_2 absorption in aqueous sodium glycinate solutions. Ind Eng Chem Res. 2007; 46: 1578-1583.
73. Ziemer SP, Niederhauser TL, Merkley ED, Price JL, Sorenson EC, McRae BR, et al. Thermodynamics of proton dissociations from aqueous glycine at temperatures from 278.15 to 393.15 K, molalities from 0 to 1.0 mol·kg^{-1}, and at the pressure 0.35 MPa: Apparent molar heat capacities and apparent molar volumes of glycine, glycinium chloride, and sodium glycinate. J Chem Thermodyn. 2006; 38: 467-483.
74. DOW™ Reverse osmosis membrane module BW30-400. Available from: https://www.dupont.com/products/filmtecbw30400.html.
75. Mona A, Sabah M, Rehab A. Influence of potassium sulfate on faba bean yield and quality. Aust J Basic Appl Sci. 2011; 5: 87-95.
76. Filmtec™ reverse osmosis membranes. Technical manual. Midland: Dow; 2010. Available from: https://www.lenntech.com/Data-sheets/Filmtec-Reverse-Osmosis-Membranes-L.pdf.
77. DOW™ Ultrafiltration module SFP-2880. Available from: https://www.lenntech.com/Data-sheets/Dow-UF-SFP-2880-L.pdf.
78. Dai Z, Deng J, Ansaloni L, Janakiram S, Deng L. Thin-film-composite hollow fiber membranes containing amino acid salts as mobile carriers for CO_2 separation. J Membr Sci. 2019; 578: 61-68.
79. Ramezani R, Mazinani S, Di Felice R. State-of-the-art of CO_2 capture with amino acid salt solutions. Rev Chem Eng. 2022; 38: 273-299.
80. Liang ZH, Rongwong W, Liu H, Fu K, Gao H, Cao F, et al. Recent progress and new developments in post-combustion carbon-capture technology with amine based solvents. Int J Greenh Gas Control. 2015; 40: 26-54.

81. Random packing vs. structured packing [Internet]. Houston: MACH. Available from: https://www.machengineering.com/random-packing-vs-structured-packing/.
82. Kister H, Gill D. Predict flood point and pressure drop for modern random packings. Chem Eng Prog. 1991; 87: 32-42.
83. Stichlmair J, Bravo JL, Fair JR. General model for prediction of pressure drop and capacity of countercurrent gas/liquid packed columns. Gas Sep Purif. 1989; 3: 19-28.
84. Billet R, Schultes M. Prediction of mass transfer columns with dumped and arranged packings: Updated summary of the calculation method of Billet and Schultes. Chem Eng Res Des. 1999; 77: 498-504.
85. Leva M. Reconsider packed-tower pressure-drop correlations. Chem Eng Prog. 1992; 88: 65-72.
86. Kister HZ, Scherffius J, Afshar K, Abkar E. Realistically predict capacity and pressure drop for packed columns. Chem Eng Prog. 2007; 103: 28-38.
87. Onda K, Takeuchi H, Okumoto Y. Mass transfer coefficients between gas and liquid phases in packed columns. J Chem Eng Japan. 1968; 1: 56-62.
88. Bravo JL, Fair JR. Generalized correlation for mass transfer in packed distillation columns. Ind Eng Chem Process Des Dev. 1982; 21: 162-170.
89. Billet R, Schultes M. Predicting mass transfer in packed columns. Chem Eng Technol. 1993; 16: 1-9.
90. Brown TR. Cost engineering: Equipment purchase cost. Chem Eng. 2019: 51-53.
91. Towler G, Sinnott R. Chemical engineering design: Principles, practice and economics of plant and process design. Burlington/San Diego/London: Elsevier; 2008.
92. Ashkanani HE, Wang R, Shi W, Siefert NS, Thompson RL, Smith K, et al. Levelized cost of CO_2 captured using five physical solvents in pre-combustion applications. Int J Greenh Gas Control. 2020;101:103135.
93. Lozowski D. The chemical engineering plant cost index [Internet]. Access Intelligence; 2021. Available from: https://www.chemengonline.com/pci-home.
94. Ashkanani HE, Wang R, Shi W, Siefert NS, Thompson RL, Smith K, et al. Effect of Power plant capacity on the CAPEX, OPEX, and LCOC of the CO_2 capture process in pre-combustion applications. Int J Greenh Gas Control. 2021; 109: 103371.
95. Wang R, Ashkanani HE, Li B, Morsi BI. Development of an innovative process for post-combustion CO_2 capture to produce high-value $NaHCO_3$ nanomaterials. Int J Greenh Gas Control. 2022; 120: 103761.
96. Commercial electricity rate in industry [Internet]. Golden: NREL; 2021 . Available from: https://www.electricitylocal.com/states/pennsylvania/industry/#ref.
97. Koronaki I, Prentza L, Papaefthimiou V. Parametric analysis using AMP and MEA as aqueous solvents for CO_2 absorption. Appl Therm Eng. 2017; 110: 126-135.
98. Xie C, Dong Y, Zhang L, Chu G, Luo Y, Sun B, et al. Low-concentration CO_2 capture from natural gas power plants using a rotating packed bed reactor. Energy Fuels. 2018; 33: 1713-1721.
99. Potassium bicarbonate handbook. Florida: Armand Products; 2021. Available from: https://www.armandproducts.com/content/pdfs/PotBiVs6.PDF.
100. Kuepper G, Thomas R, Earles R. Use of baking soda as a fungicide [Internet]. Butte: National Center for Appropriate Technology; 2001. Available from: https://web.archive.org/web/20100507163427/http://attra.ncat.org/attra-pub/bakingsoda.html.

Enjoy *JEPT* by:

1. Submitting a manuscript
2. Joining in volunteer reviewer bank
3. Joining Editorial Board
4. Guest editing a special issue

For more details, please visit:
http://www.lidsen.com/journal/jept